

Load Carrying Capacity of the Hybrid Beam

J. Václavík^{1,*}, L. Dopierała², B. Walczak², M. Hejman³

¹ *Výzkumný a zkušební ústav Plzeň s.r.o., Czech Republic*

² *Solaris Bus & Coach sp. z o.o., Poland*

³ *Fatigue Analysis RI s.r.o., Czech Republic*

* *vaclavik@vzuplzen.cz*

Abstract: Hybrid beams were designed for the local reinforcement of the bus structure. They are formed from hollow profile, CFRP plate and the foam. To verify the load-bearing capacity of the beam and the analytical and FEM calculations, several static and dynamic tests were performed. Tests on basic materials are described in this article. The goal is to determine the allowable structural stress ensuring that the plate will not be deboned during bus performance.

Keywords: bus structure; CFRP; foam; hybrid beam; adhesive joint.

1 Introduction

Carbon fibre-reinforced polymers (CFRP) are often used for strengthening of concrete and more recently steel structures in civil engineering. The use of CFRP materials was spread out also to the vehicle industry. Nowadays vehicle producers must achieve the lowest possible weight of the vehicle with a view to reducing the energy consumption and environmental impact. High interest is to use hybrid materials, which do not require modification of the vehicle production process and lead to strengthen the steel structure [1].

CFRP materials can produce a significant improvement of the local structural response through a significant increment of the local stiffness and strength. This is particular appealing for flexural strengthening at the ultimate limit state, fatigue reinforcement, strengthening against local buckling and confinement of hollow profiles. In particular, for flexural strengthening in the elastoplastic regime, the bonding of CFRP materials produces a significant increment of the plastic moment of the reinforced steel section leading to a considerable increment of the failure load.

In [3], results of some test on samples with bonded pultruded CFRP strips Sika CarboDur M514 bonded with thixotropic epoxy resin Sikadur 30 are presented. Static tests after artificial aging had shown that even if the stiffness and strength capability of the bond is not affected, the ductility of the reinforcement drops to 50%. The study also covered the surface treatment techniques, adhesive curing, and support condition under cyclic loading including fatigue performance, crack propagation, and failure modes with FE simulation. The application of CFRP strengthening composites not only delays the initial crack, reduces the crack growth rate, and extends the fatigue life, but also decreases the stiffness decay with residual deflection.

The influence of the CFRP plate end form was studied in [4]. To help maximize the capacity of bonded joints, all plate ends should implement a reverse tapered detail. Nevertheless the failure by debonding typically occurred when the peak shear stress in the adhesive reached a limiting value of.

Our effort is to improve the vehicle structure with hybrid beams, which are stiffened with CFRP plates and foam inside the hollow profiles. To verify the load-bearing capacity of the beam and the analytical and FEM calculations, several static and dynamic tests were performed. Tests on basic materials are described in this article.

2 Theory

2.1 Analytical solution

The dominant failure mode which can prevent the full load bearing capacity of the hybrid bus structure is the debonding of the CFRP plate. During the debonding process the part of the steel plate not covered by the CFRP plate undergoes plastic deformation while the other part, covered by the CFRP strips remains elastic.

An analytical formulation for prediction the failure load of steel/CFRP joints including plastic deformation of the steel was derived in [2]. Using stress based approach; the shear stress distribution close to the reinforcement ends is given by

$$\tau_{a1} = -\frac{P}{2b_a} \frac{\lambda}{(\delta + 1)} e^{-\lambda x} = \tau_{a1,\max} \cdot e^{-\lambda x}, \quad (1)$$

where

$$\delta = \frac{E_s A_s}{2E_f A_f} \quad \text{and} \quad \lambda = \sqrt{\frac{f_2}{f_1}} = \sqrt{\frac{G_a b_a}{t_a} \left(\frac{1}{E_f A_f} + \frac{2}{E_s A_s} \right)}, \quad (2)$$

where P is the loading force, b_a, t_a are CFRP width and thicknes, x is the distance of reinforced end, E_s, A_s, E_f, A_f are steel plate end CFRP plate Young's modulus and section area, G_a is adhesive sheer modulus.

The shear stress level is the indicator of unbonding the CFRP layer. The debonding failure load can be estimated as follows

$$P_{lim} = (1 - e^{-\lambda l}) \frac{-2b_a \tau_{a2,\max} \cdot (\delta + 1)}{\lambda \cdot \delta}. \quad (3)$$

An estimation of the required length l , of the adhesive joint in order to achieve a 99% of the maximum strength is $l_{\min} \geq \frac{5}{\lambda}$, which for our sample under investigations was $l_{\min} = 39$ mm.

Based on this theory the distribution of shear stress and peeling stresses in steel adhesive beginning at the CFRP end for our hybrid sample were calculated (Fig. 1).

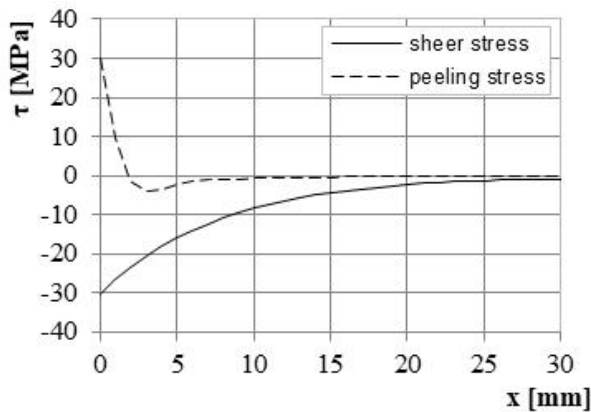


Fig. 1: Shear and peeling stress distribution in the DSR adhesive sample ($P = 60$ kN), corresponding to tensile stress $\sigma = 400$ MPa.

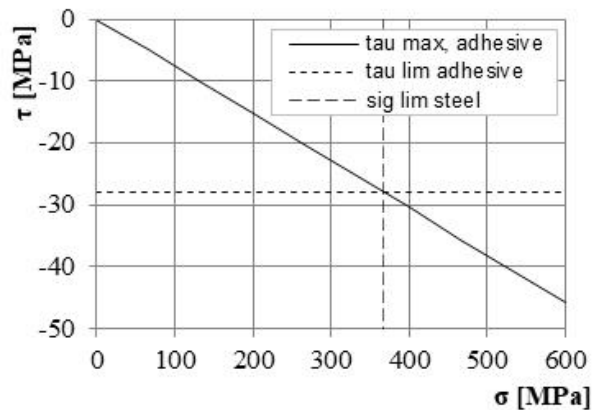


Fig. 2: Relation between shear stress in the adhesive and the tensile stress with allowable steel and adhesive stress limits.

According the linear relation between the structure tensile stress and shear stress in adhesive at the reinforced end presented in Fig. 2 it is obvious, that the maximum allowable tensile stress at the CFRP end without interface delamination can reach 370 MPa; this value is higher than the yield point of the rolled plate but lower than that of cold-drawn hollow profile used for the bus structure. The plastic joints are formed in front of the reinforcement in first case but the second case means that the CFRP reinforcement is able to accommodate the development of plastic deformation in the steel. In any case the debonding process to start at the CFRP plate ends after yielding of the steel [3].

3 Implementation

The reinforcement was made with unidirectional pultruded CFRP plates SIKA Carbodur S512 and M512, thickness 1.2 mm and length of 140 mm, $E = 165,000$ MPa and $R_m = 2,900$ MPa. CFRP plates were bonded to the stainless steel plate quality 1.4003 by an adhesive SikaPower 1277 with the thickness 0.3 mm $E = 2,000$ MPa and $R_m = 28$ MPa). Before performed tests the basic mechanical quantities of steel, CFRP plate, adhesive and foam were tested and compared with guaranteed values, given from the producer. No significant variation was

found. The special sample for tensile tests of the adhesive is given in Fig. 3. Shear test on DSL joints were also performed. The breaking sample after this test is visible in Fig. 4. The variation of measured shear strength was between 18 and 24 MPa.

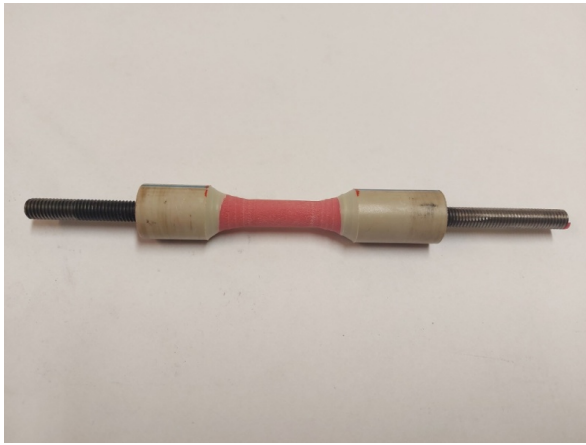


Fig. 3: Tensile sample of the adhesive, casted to the tube and subsequently turned.

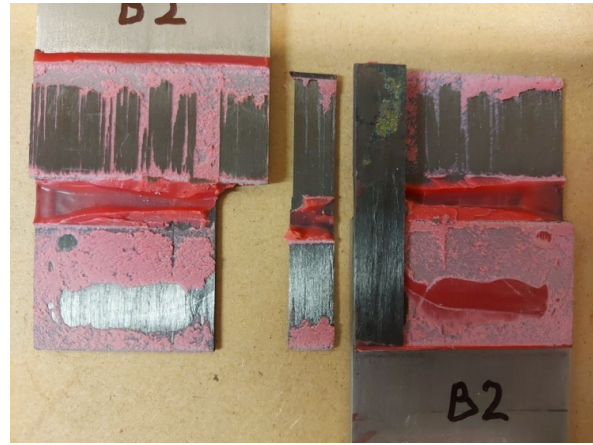


Fig. 4: Separation of double side lapped joint with Carbodur plate.

3.1 Static tensile tests of reinforced specimens

In order to validate analytical relations, the one (OSR) and double-side reinforcement (DSR) steel plates were tested under tensile tests (Fig. 5) and one-side steel plate under 3- and 4-point bending. The reinforcement for the DSR specimen was realized by two unidirectional pultruded CFRP plates Sikadur S512 and M512, with the length equal to 140 mm. All samples were made from the stainless steel quality 1.4003 as it is used for the bus structure. Flat samples made from rolled plates ($R_{p0.2} = 350$ MPa) as well as cut from hollow profile plates ($R_{p0.2} = 430$ MPa) were used for the tests. Measured maximum CFRP strains together with the maximum reached loading stress till unbonding in the distance x from the end of CFRP plate during tensile test are given in Fig. 6. Here SO corresponds to CFRP S512 bonded from one side, SB from both sides and MO CFRP M512 glued from one side.

No debonding was observed in the elastic region of the steel during tensile tests. With large stress the steel undergoes large plastic deformation outside the CFRP (tear about 20 mm of the CFRP end) with small CFRP debonding of some millimeters.



Fig. 5: DSR specimen under static tensile test.

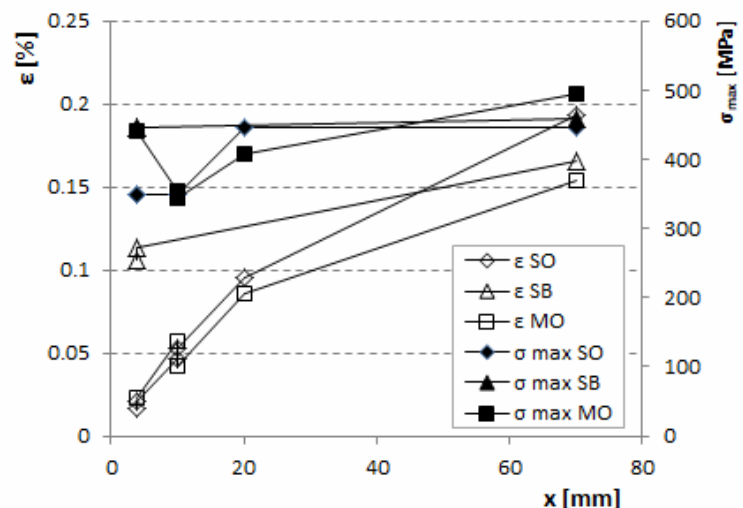


Fig. 6: Maximum CFRP strains and corresponding steel stresses at the moment of CFRP plate unbonding as a function of the distance of the CFRP end.

The comparison of stresses in the middle part of the CFRP and the middle part of steel, opposite to the CFRP for SO specimen is provided in the Fig. 7. It is clearly visible, that the stress transferring by CFRP is much lower, than the stress in the steel (from 35% at beginning of the loading to 65% after the yield point). This is not caused only with the different elastic moduli of steel and CFRP. The measured strains at CFRP and steel are not the same which is caused due to the bending of the sample (bending is worst in the elastic part of the loading curve).

From this point of view it can be concluded, that steel stress is nearly the same as the total stress (Fig. 7, green and black curves) and that the CFRP does not lower the stress substantially. However the advantage of the CFRP plate is obvious – keeps of the high plastic deformation of the sample in the area, where it is glued. The theoretical values of stress in the CFRP and steel were calculated using the total test force, elastic moduli and cross sections of the sample and the CFRP plate and are also given in Fig. 7. These stresses differ not so much, as measured elastic modulus of the steel was low and no bending was considered.

CFRP debonding occurs at 0.38% steel strain, which corresponds to the apparent tensile stress 800 MPa.

The distribution of the longitudinal strain in the CFRP plate from the beginning of the plate to the plate center is shown in Fig. 8. The different curves characterize the different time sections of the loading history up to reaching the yield point. Each cut is specified with the reached testing stress. The curves are normalized to the strain in the middle of the sample. It is interesting, that at the beginning of the loading the stress maximum is not in the middle of the CFRP but closer to the end of the CFRP (here at the distance of 20 mm). The stress does not transferee whole the CFRP plate. During increasing the force the stress is distributed in the CFRP plate according the theoretical assumptions.

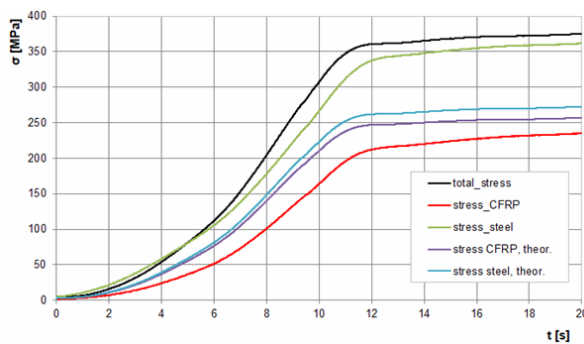


Fig. 7: Total loading stress in the sample, measured stress time history at the center of the sample on CFRP and on steel and theoretical distributed stresses here computed using the total stress.

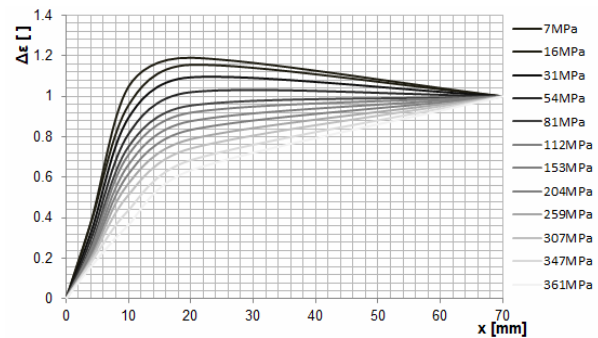


Fig. 8: The distribution of the longitudinal strain in the CFRP plate from the beginning of the plate to the plate center.

3.2 FEM calculations of tensile tests

FEM calculations of the reinforcement specimen was performed in software ANSYS. The linear isotropic material properties were considered according to chapter 3. Quadratic hexagonal elements were used for steel plate, glue and CFRP plate. Three test specimens were modeled. Steel plates with glued CFRP plate Sikadur S512 on one side SO, on both side SB and CFRP plate Sikadur M512 on one side MO. The model was loaded by force 1 kN and scaled for loading force at the moment of CSRP plate unbonding, see Fig. 9. The force corresponding to the total stress see Tab. 1.

Tab. 1: Loading Force at the moment of CSRP plate unbonding.

	Sigma [MPa]	Force [N]
SO	350	52,500
SB	455	68,250
MO	345	51,750



Fig. 9: Loading and boundary conditions of the $\frac{1}{4}$ test specimen FEM model.

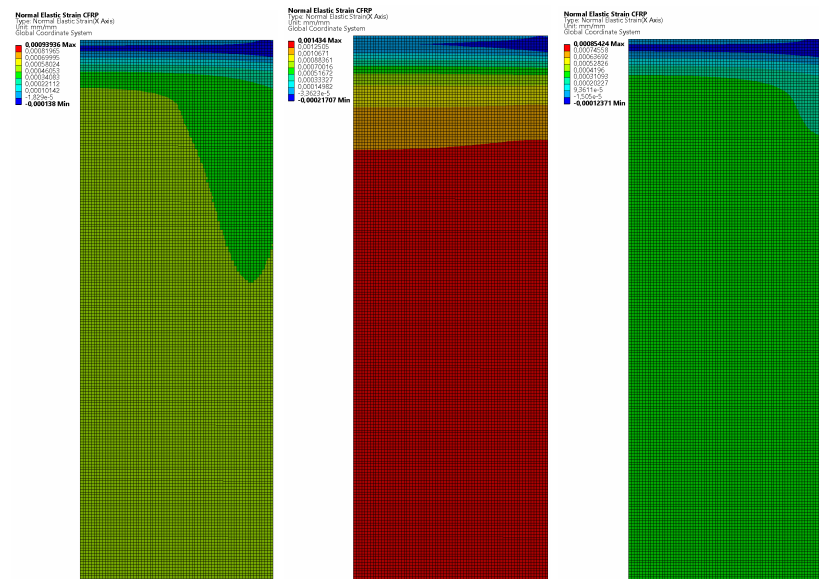


Fig. 10: Field of strain ε [%] in CFRP strap of SO, SB and MO test specimens at the moment of CSRP plate unbonding.

It is possible to compare evaluated strain in Fig. 11 with result of measurement in Fig. 6. The test specimens SO and MO have approximately three time higher strain then in calculations. The reason can be the effect of debonding of CFRP strap or simplified FEM modeling.

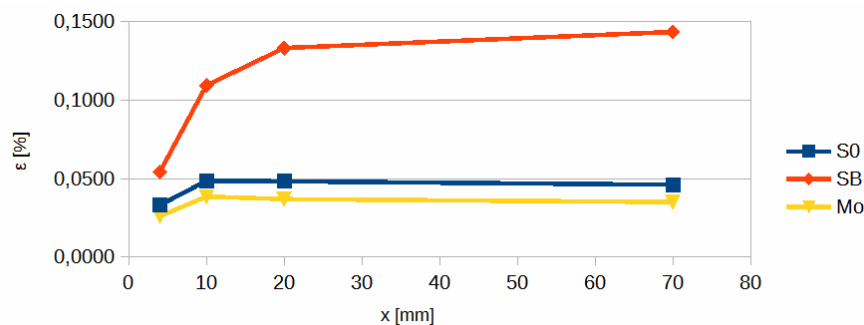


Fig. 11: Strain ε [%] of SO, SB and MO test specimens at the moment of CSRP plate unbonding as a function of the distance of the CFRP end.

To achieve a suitable approximation of SO and MO tests, it is necessary to ensure better measurement of the characteristics of the materials used and implement them in the FEM model.

3.3 Static bending tests of reinforced specimens

3-point and 4-point bending test was realized with the rectangular steel 1.4003 beam with glued CFRP plate of the length 180 mm from the bottom.

During increasing of the deflection, plastic joints were formed in the steel in the area behind the end of the CFRP strips with where very high strain. Plastic strains were also measured on the upper side of the steel above the glued CFRP plate between the applied force pair, but no visual deflection was observed here. The separation of the strip occurred at a steel strain at the end of the strip at $\varepsilon = 3,000 \mu\text{m}\cdot\text{m}^{-1}$, which corresponds to an apparent stress of about 600 MPa.

In the elastic state the sample stiffness with CFRP plate has increased of about 65 %. Due to the shift of the beam neutral axis the strain on the beam upper part drops of about 14 %. However in the elastic plastic state the highest strains were comparable.



Fig. 12: Four-point bending test of steel plate with glued CFRP plate. Plastic joints on both reinforced ends and visible debonding of the CFRP plate.



Fig. 13: Detail of debonding of the reinforce end after plastic deformation of the beam.

4 Conclusion

Results of static tests of hybrid beam individual components were in agreement with producer datasheets. In elastic state the improvement of sample stiffness was substantially improved. After reaching the yield point the plastic deformation occurs in areas not covered with CFRP plate. The conclusion is that the reinforcement ends have not end in the area with high stresses. However it was proved that the CFRP reinforcement is able to accommodate the development of plastic deformation in the steel.

Acknowledgement

The article has originated in the framework of M-ERA.NET call 2019 and was supported with Technological Agency of Czech Republic under the No. TH71020003.

References

- [1] J. Korta, T. Uhl, Multi-material design optimization of a bus body structure, *J KONES Powertrain Transp* 2013, 139–146.
- [2] M. Bocciarelli, P. Colombi, G. Fava, C. Poggi, Prediction of debonding strength of tensile steel/CFRP joints using fracture mechanics and stress based criteria, *Engineering Fracture Mechanics* 76 (2009) 299–313.
- [3] M. Bocciarelli, P. Colombi, G. Fava, G. & C. Poggi, Some issues on the strengthening of steel structures with fibre-reinforced polymer materials, *Australian Journal of Structural Engineering*, Vol. 15, No. 4, October 2014, 337–354.
- [4] M. Dawood, S. Rizskala, Bond and splice behavior of CFRP laminates for strengthening steel beams, <https://www.researchgate.net/publication/252419022>.